Improved Multiple-Particle Tracking for Studying Flows in Multiphase Systems

Z. Yang
Dept. of Chemical Engineering, School of Engineering, University of Birmingham, Birmingham B15 2TT, U.K.

X. Fan
School of Physics and Astronomy, University of Birmingham, Birmingham B15 2TT, U.K.

P. J. Fryer
Dept. of Chemical Engineering, School of Engineering, University of Birmingham, Birmingham B15 2TT, U.K.

D. J. Parker
School of Physics and Astronomy, University of Birmingham, Birmingham B15 2TT, U.K.

S. Bakalis
Dept. of Chemical Engineering, School of Engineering, University of Birmingham, Birmingham B15 2TT, U.K.

DOI 10.1002/aic.11224
Published online June 20, 2007 in Wiley InterScience (www.interscience.wiley.com).

Positron Emission Particle Tracking is a powerful and noninvasive technique and has been successfully used in a wide range of fundamental research and industrial applications. However, it is only capable of following a single tracer. This article presents a Multiple-Positron Emission Particle Tracking technique for tracking two freely moving particles in opaque systems and its application. The developed technique has been validated through tracking two stationary particles and two moving particles, respectively. The results showed that it is a reliable technique and can be potentially used to acquire more comparative information, such as the interactions and relative motions of particles with different sizes, densities, and material textures in multiphase systems. Tracking two polyethylene particles, labeled using ^{18}F, in a cylindrical fluidized bed has been given as an example. The information obtained provides significant insights into phenomena in flow and mixing processes. © 2007 American Institute of Chemical Engineers *AIChE J,* 53: 1941–1951, 2007

Keywords: PEPT, multiple-positron emission particle tracking, identification, location algorithm, fluidization

Introduction

The technique of Positron Emission Particle Tracking (PEPT) has been developed at the University of Birmingham for tracking a single particle accurately and noninvasively for various applications in engineering and science. The technique involves a positron camera, a labeled tracer particle,[1,2] and a location algorithm used for calculating the tracer location and speed. The camera consists of two position-sensitive detectors, each with an active area of 500 × 400 mm^2, mounted on either side of the field of view, and is used to detect pairs of 511 keV γ-rays. The tracer particle is labeled

Correspondence concerning this article should be addressed to S. Bakalis at s.bakalis@bham.ac.uk.

using a radionuclide, which decays by β^+ decay with the emission of a positron. Each positron rapidly annihilates with an electron, giving rise to a pair of 511 keV γ-rays, which are emitted almost exactly back-to-back. The two γ-rays are simultaneously detected in the two detectors and define a trajectory passing close to the source. Early trials of this PEPT technique were reported by Bemrose et al.[3] in 1988. The technique was then revived by Parker et al.[4] in 1993, using an improved location algorithm, with the result that significant improvements in location accuracy have been achieved. Parker et al.[4] pointed out that all the uncorrupted γ-ray trajectories for a given set of events should meet (to within the resolution of the camera) at a point in space, which is the location of the particle. They went on to develop the location algorithm. The location algorithm calculates the point, which minimizes the sum of perpendicular distances to the various trajectories. In practice many of the detected events are corrupt because (i) one or both of the pair of γ-rays have undergone Compton scattering prior to detection or (ii) the two detected γ-rays were not in fact a pair of 511 keV photons originating from the same positron annihilation event. Thus, the developed location algorithm discards these corrupt events, whose trajectories are broadcast randomly in space, and do not in general pass close to the true particle location, and then recalculates the location using just the uncorrupted events. From successive locations, the velocity of the labeled particle can be found[5] as it passes through the view of the camera.

Because γ-rays can penetrate a considerable thickness of material, PEPT offers several advantages for providing an insight into flow and mixing processes inside real plant equipment without disturbing the process. In contrast with optical tracking techniques,[4] which are necessarily limited to transparent systems and suffer rather low temporal resolution [for example, Particle Imagery Velocimetry (PIV), typically 15 Hz for digital PIV], the PEPT has high resolution, a moving particle at a speed of 500 mm/s can be located 60 times per second. The PEPT has opened up a host of novel fields of study. For the past 10 years, the PEPT technique has been used to study a wide range of engineering processes[6–17] by a number of research groups.

One drawback of the PEPT technique is that it is only capable of following a single tracer at any one time. There are a number of situations where it would be valuable to track more than one particle to study the interactions and relative motions of particles within a process. For example:

- In the pharmaceutical industry,[18] the slightest changes in the ingredient properties or the process operating conditions in the manufacture of a drug can have a huge impact on its quality. It is then of paramount importance to understand the physical phenomena that govern the flow and mixing of solid ingredients involved in the manufacturing process. Tracking multiple particles will provide an insight into the phenomena and enable researchers to obtain a better understanding of physical processes.
- In the titanium refining industry,[19] the refining process begins in a fluidized bed, with the chlorination of titanium-rich rutile ore. Chlorine gas is bubbled up through a bed of rutile and coke. Thorough mixing of the three reactants is important to the yield and reaction rates of the system. By tracking the two solid reactants, mixing and segregation phenomena will be more fully understood and more accurately predicted.
- In the chemical industry,[20–22] many processes involve multicomponent mixtures. To study mixing patterns and mechanisms, tracking two particles could provide information about the uniformity of the mixture and information on relative motions, which could be helpful in understanding mixing mechanisms.

Other applications of tracking multiple particles include reactor engineering[23] and validation of Discrete Element Methods.[10]

A Multiple-PEPT was developed by Yang et al. in 2006.[24] It was used to observe the rotation of a large particle via tracking three small positron emitting tracers mounted, with fixed separation distances, on the surface. The technique has been successfully used to study the rotational and translational behaviours of a large particle in a multiphase flow. This technique has been further improved to track multiple freely moving particles recently. This article systemically describes the improved Multiple-PEPT and its application in real systems. The potential applications of the improved Multiple-PEPT are illustrated through tracking two polyethylene particles, labeled using ^{18}F, in a cylindrical fluidized bed. The information obtained provides significant insights into phenomena in flow and mixing processes.

Multiple-PEPT

As previously described, the γ-rays are emitted in a pair and almost exactly back-to-back. The two γ-rays are simultaneously detected by the two detectors. All γ-ray trajectories from a particular tracer particle should meet (to within the resolution of the camera) at a point in space, which is the location of the tracer. Figure 1 shows 100 γ-ray trajectories from an example of two labeled tracers with a separation distance of 20 mm and different activities (Tracer 1: 362 μCi and Tracer 2:176 μCi) in the field of view of the detectors over a 2.5-ms period. In the previous Multiple-PEPT,[24] the particles are assumed to be kept at a fixed distance within 25 mm at all times. When the tracers are labeled with different radioactivity levels, the stronger tracer has a higher γ-ray density and a higher data logging rate. Thus, the first point,

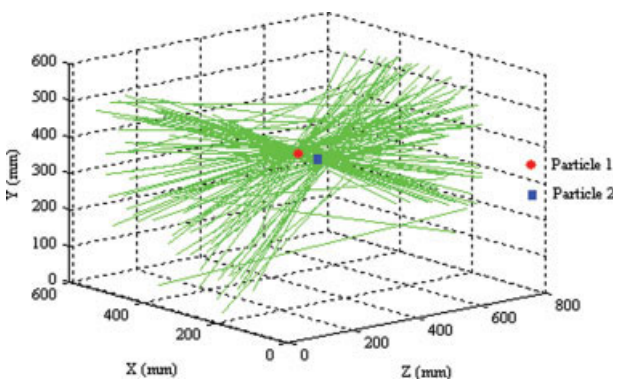

Figure 1. 100 γ-ray trajectories from the camera for two particles over a 2.5-ms period.

[Color figure can be viewed in the online issue, which is available at www.interscience.wiley.com.]

which minimizes the sum of perpendicular distances to the various trajectories, will be close to the stronger tracer for a given set of events. After removing the furthest trajectories, the minimum distance point, recalculated using the remaining subset, will be closer to the stronger tracer. The iteration procedure continues until the tracer is calculated using just the uncorrupted events from the stronger tracer. After the stronger tracer is located, the trajectories from this tracer should be removed from the dataset. The location of the second tracer is then calculated from the remaining dataset in a similar way.

However, if the previous Multiple-PEPT[24] is used for tracking multiple freely moving particles, there are several questions in the procedure, such as,

- How many trajectories should be removed after the first tracer is located?
- What is the optimum sample size for calculating the tracer locations when the tracers with different radioactivity are moving freely at different speeds?
- How does the data logging rate relate to the radioactive level?

Furthermore, in the previous Multiple-PEPT,[24] the particle identification is based on the numbers of valid trajectories in the located positions, i.e., the higher number of valid γ-ray trajectories in the located position is assumed to correspond to the stronger tracer, where the valid trajectories were defined as the trajectories passing close to the located tracer within 5 mm. However, the data logging rate decreases significantly from the center towards the edges of the detectors for the specific camera. Therefore, the previous particle identification is not suitable for multiple freely moving particles. The stronger tracer with a higher γ-ray density does not always have a higher data logging rate and can not always be found first. In practice, the tracer which has a higher data logging rate is located first, and the data logging rate depends on its position in the field of view of detectors and the labeled radioactivity. To overcome this problem, the tracers should be identified as stronger or weaker. Thus, the questions arising from tracking multiple freely moving particles are (i) how the data logging rate and the number of valid γ-ray trajectories depend on the tracer position in the field of view of detectors, (ii) how the tracers can be identified as stronger or weaker, (iii) how the location algorithm can be improved to accurately calculate the positions of the tracers in freely moving situations, and (iv) how the time at each location can be reconstructed. The improved Multiple-PEPT will be established from the following investigations.

Investigation into the variation of the data logging rate as a function of the labeled radioactive level

To investigate the relationship between the data logging rate and the labeled radioactivity level, a series of tracer particles with different radioactivity were mounted at the center of the field of view of detectors in turn, as shown in Figure 2. Approximately 2 min data were recorded for each tracer particle. The variation of the data logging rate as a function of the labeled radioactivity level is shown in Figure 3. The results indicate that the data logging rate is directly proportional to the labeled radioactivity level when the tracers are placed at the center of the field of view of detectors, i.e., the numbers of trajectories at the center are directly proportional to the labeled radioactivity levels.

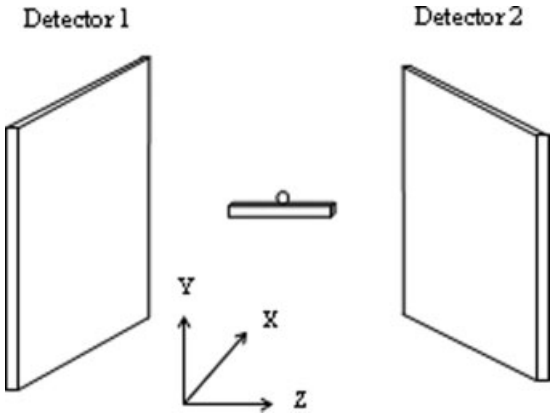

Figure 2. Schematic diagram of PEPT for a single stationary particle.

Investigation into the variations in the data logging rate and the fraction of valid trajectories as a function of particle position

The variations in the data logging rate and the fraction of valid trajectories as a function of particle position were investigated using ^{18}F labeled particles with an activity of $\sim$114 μCi and a detector separation of 600 mm. The particle was mounted in the field of view of detectors at a series of locations along the x-, y- and z-axes, as shown in Figure 2. Each run took 2 min for data collection, and the location was calculated from a sample size of 500 events. To test the consistency and reliability of the tracking technique, the 3D standard deviation of locations was also investigated when the tracer was in different positions.

The data logging rate was calculated by:

$$\frac{\text{Number of recorded events (in the located position)}}{\text{Number of recorded events (at the center)}},$$

and the fraction of valid trajectories by:

$$\frac{\text{Number of valid trajectories}}{\text{Sample size}}$$

Figure 4A shows that the data logging rate varies significantly from the center towards the edges of the detectors if

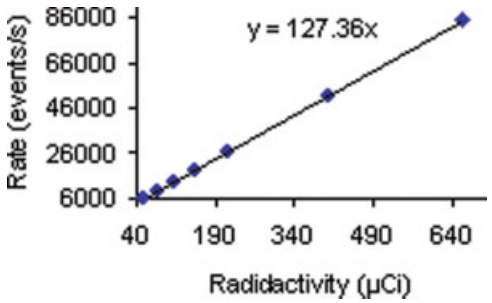

Figure 3. The variation of the data logging rate as a function of the labeled radioactivity.

[Color figure can be viewed in the online issue, which is available at www.interscience.wiley.com.]

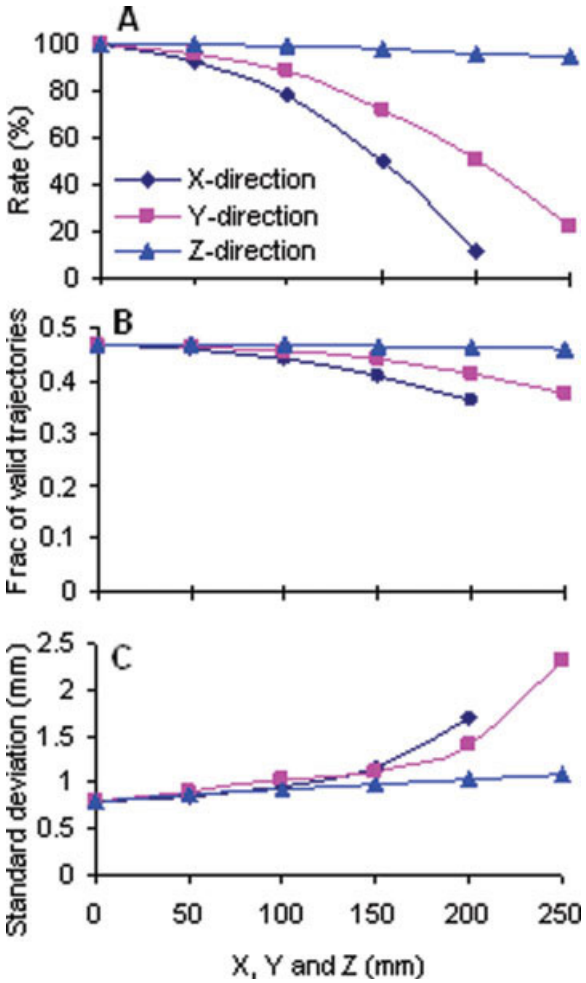

Figure 4. A–C show the variation in the data logging rate, the variation in the fraction of valid trajectories, and the 3D standard deviation achievable, respectively—all as a function of particle position along the three axes.

[Color figure can be viewed in the online issue, which is available at www.interscience.wiley.com.]

the data logging rates are: 100% at the center, then decrease to 12% at 200 mm off-center in x-direction; 22% at 250 mm off-center in y-direction; and 94% at 250 mm off-center in z-direction for the labeled particle. The data logging rate from a quadratic approximation to the curves in Figure 4A in the location (x, y, z) is:

$$\text{Rate} \equiv \frac{\psi(x,y,z)}{\psi_0} = \left[1-2\left(\frac{x}{Dx}\right)^2\right]\left[1-2\left(\frac{y}{Dy}\right)^2\right]\left[1-2\left(\frac{z}{Dz}\right)^2\right] \quad (1)$$

where $\psi(x, y, z)$ is the number of trajectories passing close to the location (x, y, z), ψ_0 is the number of trajectories at the center(x_0, y_0, z_0), and ψ_0, $Dx, Dy,$ and Dz are supplied for a particular nuclide and scattering environment.

Figure 4B shows that the labeled particle gives about 46% valid trajectories in total at the center; the valid trajectories will slightly decrease, while the particle is closer to the edges of the field of view, falling from roughly 46% at the center to 36% at 200 mm off-center in x-direction, 37% at 250 mm off-center in y-direction, and 45% at 250 mm off-center in z-direction. The fraction of valid trajectories from a quadratic approximation to the curves in Figure 4B around the location (x, y, z) is:

$$f(x,y,z) \equiv \frac{\text{Number of valid trajectories}}{\text{Sample size}} = f_0\left[1-0.5\left(\frac{x}{Dx}\right)^2\right]\left[1-0.5\left(\frac{y}{Dy}\right)^2\right]\left[1-0.5\left(\frac{z}{Dz}\right)^2\right] \quad (2)$$

where f_0, $Dx, Dy,$ and Dz are supplied for a particular nuclide and scattering environment, and f_0 is the fraction of valid trajectories at the center (x_0, y_0, z_0) of the field of view.

Figure 4C shows that the ability to locate the particle accurately within a fixed sample size of the data is reduced towards the extremes of x or y because the overall data rate falls significantly, and the quality of the data becomes poorer, but accurate location is possible over most of the field of view of the detectors, i.e., the established Eqs. 1 and 2 can be used to precisely calculate the data logging rate and the fraction of valid trajectories over most of the field of view.

Investigation into the optimum sample size

The selection of sample size is very complex, and determined by the tracer radioactivity and speed. It plays an important role in location accuracy. Therefore, two experiments were performed to optimize the sample size; one is for tracking a stationary particle labeled with different radioactivity, and the other for tracking a moving particle labeled with different radioactivity and moving at different speeds. Each run took 2 min as mentioned earlier.

For the stationary particle, the tracers labeled with radioactivity level over a range from 50 to 655 μCi were placed at the center of the field of view of the detectors in turn, as shown in Figure 2. The 3D standard deviations of location tracking as a function of the sample size are calculated for each test. Because of very similar trends for the tracers with different radioactivity levels, only the 3D standard deviation for a radioactivity of 210.3 μCi is shown in Figure 5. The results show that the tracking accuracy can be improved as the sample size increases for a stationary particle. As expected, more information results in more accurate location.

For moving particle tracking, one tracer was fixed on a turntable at a radius of 106 mm. The turntable was placed at the center of the field of view of the detectors, and rotated at a constant speed for each run. To investigate the effect of radioactivity and particle speed on the optimum sample size, the rotating speeds of the turntable varied from 2 to 45 rpm, the particle speeds varied from 22 to 500 mm/s, and the tracer was labeled with 362 and 176 μCi, respectively.

Figure 6 shows that the optimum sample size varies with the tracer speed and radioactivity. When the tracer particle speed is high, a small sample size should be selected to give more locations to smooth the motion trajectory. If a tracer has a higher radioactivity, the γ-ray events generated in the same period is larger; the optimum sample size therefore can

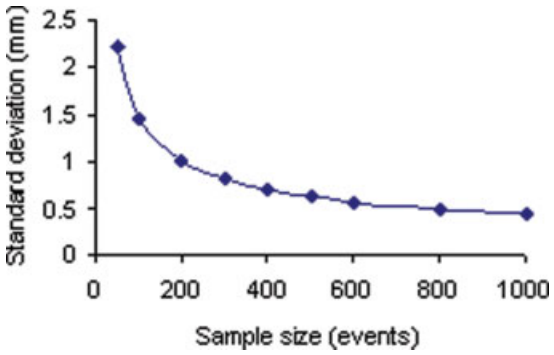

Figure 5. The 3D standard deviation as a function of the sample size.

[Color figure can be viewed in the online issue, which is available at www.interscience.wiley.com.]

be big to obtain more accurate locations. For this specific camera, the maximum useful count rate is around 100 k events/s and the corresponding maximum radioactivity is about 785 μCi estimated by the equation ($y = 127.36x$) in Figure 3. In practice, the selection of radioactivity is determined by an available labeled tracer.

It should be noted that the ratio of the optimum sample sizes (2.0) is equal to the ratio of their radioactivity levels (362/176) for the two tracers at any speed from Figure 6. Thus for any radioactivity level, the optimum sample size can be calculated from the equations in Figure 6. For example, from the equation$y = -1.5347x + 1076.1$, the optimum sample size can be described as follows.

$$\text{Sample size} = \frac{C(-1.5347v + 1076.1)}{362} = C(-0.00424v + 2.97) \quad (3)$$

where C is radioactivity (μCi), and v particle speed (mm/s).

The optimum sample size for multiple moving particles can be approximately estimated by Eq. 3, based on the radioactivity of weaker or/and fast tracer particle.

Location algorithm

From the earlier investigations, the data logging rate varies with the labeled radioactivity level and the position of a tracer. Thus, for the two tracers labeled with different radioactive levels, the tracer with a higher data logging rate would be located first using single particle tracking,[4] while the trajectories from the remaining tracer are regarded as corrupt trajectories. Trajectories passing close to the located tracer are then removed from the dataset. The location of the second tracer is then calculated in a similar way. After the tracers are located, the tracers should be identified as stronger or weaker.

For a selected set S of sequential γ-ray trajectories $L_1, \ldots, L_N$, which are logged data from the camera, the sum of distances from any point (x, y, z) to the γ-ray trajectories can be stated as follows.

$$D_s(x, y, z) = \sum_s \delta_i(x, y, z) \quad (4)$$

where $\delta_i(x, y, z)$ is the distance of the ith trajectory from the point (x, y, z).

To get the minimum sum of distances, the minimum solution must be obtained by

$$\begin{cases} \dfrac{\partial D_s(x,y,z)}{\partial x} = 0 \\ \dfrac{\partial D_s(x,y,z)}{\partial y} = 0 \\ \dfrac{\partial D_s(x,y,z)}{\partial z} = 0 \end{cases} \quad (5)$$

From Eq. 5, the minimum distance point (x_0, y_0, z_0) can be obtained as the first approximation. The mean deviation of these trajectories from the minimum distance point is then

$$d_s(x_0, y_0, z_0) = D_s(x_0, y_0, z_0)/N(S) \quad (6)$$

where $N(S)$is the number of events in the set S.

Then the corresponding distance $\delta_i(x_0, y_0, z_0)$ of the ith trajectory from the point (x_0, y_0, z_0) is calculated. The trajectory for which $\delta_i(x_0, y_0, z_0)$ is larger than $k\, d_s(x_0, y_0, z_0)$ is discarded, where k is a fixed parameter. This leaves a subset S_1 of events and a new (smaller) mean deviation $d_{s1}(x_1, y_1, z_1)$, from which an improved location (x_1, y_1, z_1) of the tracer with a higher data logging rate is calculated. The algorithm proceeds by iteration in this way, selecting subsets S_2, S_3, etc. The parameter k determines the rate at which trajectories are discarded. The optimum value of k lies somewhere between 1 and 1.5.[4,24]

Supposing that the parameters f_1 and f_2 are the first- and second-tracer fractions of the initial trajectories, respectively, and another parameter ρ is the fraction of the desired trajectories in the entire original set S, the iteration continues until only a specified fraction f of the initial trajectories remains, i.e., the process is terminated at step n, where $N(\mathrm{S}_n) = fN(S)$ and $f = \rho f_1$. The best value of the parameter[4] ρ is between 0.20 and 0.33. The parameters f_1 and f_2 are related to the data logging rates of tracers. The detail about the parameters f_1 and f_2 will be described later.

After the tracer with a higher data logging rate is located, the trajectories from the located tracer are removed from the dataset. As many as possible of the trajectories from the first tracer should be discarded from the dataset, so that the tracking for the second tracer has minimal contamination from the

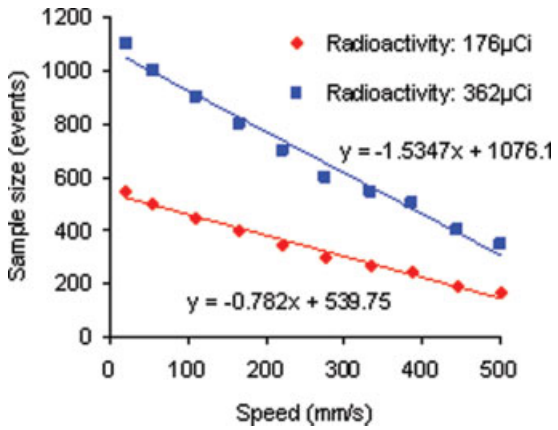

Figure 6. The variation in the optimum sample size as a function of particle speed.

[Color figure can be viewed in the online issue, which is available at www.interscience.wiley.com.]

first tracer. The fraction of discarding trajectories (β) from the first located tracer will be investigated below. After removing the trajectories from the dataset, the location of the second tracer is then calculated from the remaining dataset in a similar way.

Particle identification—γ-ray density detection

As mentioned earlier, the tracers have to be identified as stronger or weaker to safeguard the track after the tracers are located. For the two freely moving particles, they can not be directly identified by the numbers of valid trajectories from the tracers. However, from the established Eq. 2 and the numbers of valid trajectories from the tracers, the numbers of trajectories can be calculated in the located positions; and then from the established Eq. 1, the numbers of trajectories converted to their equivalents at the center of the field of view of the detectors, where the numbers of trajectories are directly proportional to their labeled radioactivity levels, can be calculated, resulting in particle identification.

For the located tracer, the number of the valid trajectories $\phi(x,y,z)$ passing close to the located position (x,y,z) within 5 mm can be calculated as follows:

$$\begin{cases} j(i)=1 \quad (\delta_i(x,y,z)\le 5, \quad i=1,2,...,N) \\ \phi(x,y,z)=\sum_1^N j(i) \end{cases} \tag{7}$$

The number of trajectories in the located position (x,y,z) from Eqs. 2 and 7 is:

$$\begin{aligned} m &= \phi(x,y,z)/f(x,y,z) \\ &= \phi(x,y,z)\Big/\left\{f_0\left[1-0.5\left(\frac{x}{Dx}\right)^2\right]\left[1-0.5\left(\frac{y}{Dy}\right)^2\right]\right. \\ &\qquad \left.\times\left[1-0.5\left(\frac{z}{Dz}\right)^2\right]\right\} \end{aligned} \tag{8}$$

Supposing the parameters m and n are the numbers of trajectories for the first and the second tracers in their located positions, respectively, m and n can be obtained from Eq. 8, and then the fractions of trajectories of the first and the second tracers can be calculated as follows:

$$f_1=\frac{m}{m+n} \tag{9}$$

$$f_2=\frac{n}{m+n} \tag{10}$$

To identify which tracer is the stronger one, the numbers of trajectories from the tracers should be compared in the same position, for example at the center of the field of view. For the position (x,y,z) of the located tracer, the number of trajectories is converted to its equivalent (m_0) at the center, and can be described as follows, from Eq. 1.

$$m_0=m\Big/\left\{\left[1-2\left(\frac{x}{Dx}\right)^2\right]\left[1-2\left(\frac{y}{Dy}\right)^2\right]\left[1-2\left(\frac{z}{Dz}\right)^2\right]\right\} \tag{11}$$

From Eq. 11, the numbers of trajectories converted to their equivalents at the center can be calculated for the located tracers, and the higher number of trajectories converted will correspond to the stronger tracer.

Time reconstruction

The final outcome is that the subsets S_{F1} and S_{F2} of trajectories are selected from the original set, from which the locations of particles 1 and 2, during the time interval covered by these subsets, are calculated as their minimum distance points (x_{F1}, y_{F1}, z_{F1}) and (x_{F2}, y_{F2}, z_{F2}), respectively. As in the previous Multiple-PEPT,[24] each event L_i has its time of measurement t_i recorded, and the location thus arrived at is considered to represent the particles' position at time

$$t=\frac{1}{N_F}\sum_{S_F} t_i \tag{12}$$

where $N_F \equiv N(S_F)$ is the number of trajectories in the final subset, and$S_F = S_{F1} \cup S_{F2}$. Having located the particles once, the new set starts immediately after the last γ-ray trajectory actually used in the previous final subset S_F.

Test of the Multiple-PEPT Algorithm

The accuracy of the Multiple-PEPT is evaluated by the location and speed errors in the results for moving particles. For stationary particles, the precision of multiple-particle tracking is validated by its consistency through the standard deviation of measurements.

$$\text{rms location error}_{\text{particle } k} \equiv \tilde{p}_k = \sqrt{\frac{\sum_{i=1}^N\left[\left(\hat{x}_k^i-x_k^i\right)^2+\left(\hat{y}_k^i-y_k^i\right)^2+\left(\hat{z}_k^i-z_k^i\right)^2\right]}{N}} \tag{13}$$

$$\text{rms speed error}_{\text{particle } k} \equiv \tilde{v}_k = \sqrt{\frac{\sum_{i=1}^N\left[\left(\hat{v}x_k^i-vx_k^i\right)^2+\left(\hat{v}y_k^i-vy_k^i\right)^2+\left(\hat{v}z_k^i-vz_k^i\right)^2\right]}{N}} \tag{14}$$

$$x\text{−Position deviation}_{\text{particle } k} \equiv \sigma_{xk} = \sqrt{\frac{\sum_{i=1}^N\left(\hat{x}_k^i-\frac{\sum_{i=1}^N \hat{x}_k^i}{N}\right)^2}{N}} \tag{15}$$

$$\text{Location deviation}_{\text{particle } k} \equiv \sigma_k = \sqrt{\sigma_{xk}^2+\sigma_{yk}^2+\sigma_{zk}^2} \tag{16}$$

where $\hat{x}_k^i$ is the position of x of particle k at time i from the Multiple-PEPT; and x_k^i is the actual value.

To test the Multiple-PEPT technique, two examples have been performed, one for tracking two stationary particles, and the other for tracking two moving particles as follows.

Tracking for stationary particles

Example 1: Two Stationary Particles. The two tracer particles were fixed on a metal bar, on which the separation dis-

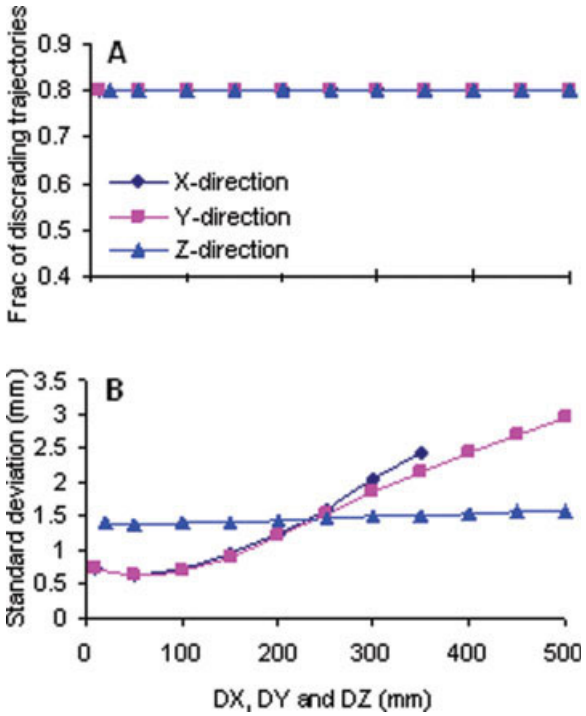

Figure 7. A and B show the optimum fraction of discarding trajectories and the achievable 3D standard deviation, respectively—all as a function of the distance between the two particles along the three axes.

[Color figure can be viewed in the online issue, which is available at www.interscience.wiley.com.]

tance of particles could be adjusted. The bar was mounted in the field of view of the detectors with different orientations for a series of experiments. The separation distance of particles was varied over the range from 10 to 500 mm. To validate the technique, the test of its consistency through the standard deviation of locations was applied. Each run took 2 min as described earlier. The locations were calculated from a sample size of 500 events. The tracers were labeled with ^{18}F, with radioactivity of 210 and 100 μCi, respectively.

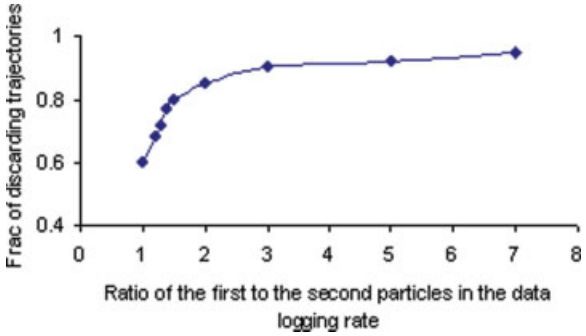

Figure 8. The optimum fraction of discarding trajectories as a function of the ratio of the first to the second particles in the data logging rate.

[Color figure can be viewed in the online issue, which is available at www.interscience.wiley.com.]

As mentioned above, after the first tracer is located, the trajectories from the located tracer will be discarded from the dataset. If the trajectories are removed properly, the second tracer will be located accurately; otherwise, the location of the second tracer would be contaminated by the trajectories from the first tracer, leading to loss of track. As is well known, the quality of the tracer location relies on its signal-to-noise ratio, thus the optimum fraction of discarding trajectories from the first tracer relates to the ratio of the data logging rates of the tracers. The other factor that could influence the optimum fraction of discarding trajectories is the distance between the tracers.

To find out how the optimum fraction of discarding trajectories varies as the distance changes between two particles, the distance was adjusted along three axes, and the particles were placed with central symmetry to keep the same ratio in their data logging rates. The standard deviations for the two particles are similar and thus only the 3D standard deviation for the stronger one is displayed in Figure 7B.

The results show that the optimum fraction of discarding trajectories keeps a constant (0.8), as shown in Figure 7A, while the distance changes between the two particles, where the ratio of the first to the second particles in the data logging rate is unchanged. The results indicate that the optimum fraction of discarding trajectories has nothing to do with the distance between the two particles. The results also show that as the particle is further away from the center, the standard deviation increases, but is reasonable over most of the field of view of detectors, as shown in Figure 7B.

To obtain the optimum fraction of discarding trajectories when the ratio in the data logging rate of two particles changes, the stronger tracer was mounted at the center and the weaker tracer was placed in different positions; and then the weaker tracer was fixed at the center and the stronger tracer was placed in different positions, thus the ratio in the data logging rate of two particles varied.

Figure 8 shows that the optimum fraction of discarding trajectories increases as the ratio of the first to the second located particles in the data logging rate increases. As well expected, when the data logging rate of the first particle is

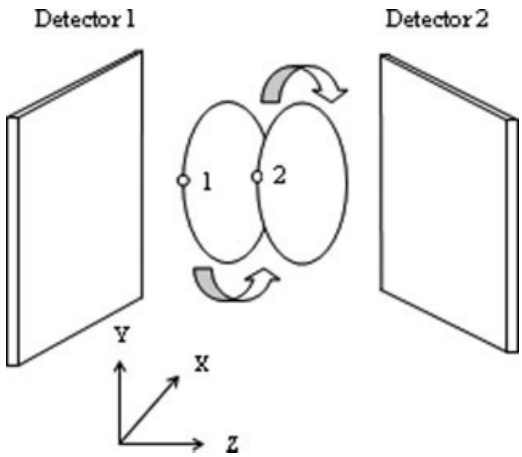

Figure 9. Schematic diagram of multiple-positron emission particle tracking for two moving particles.

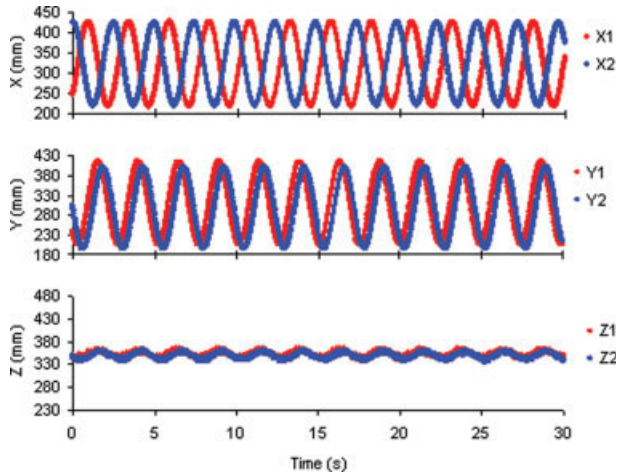

Figure 10. Example of location data for Particles 1 and 2 from multiple-positron emission particle tracking over a 30-s period.

[Color figure can be viewed in the online issue, which is available at www.interscience.wiley.com.]

the same as that of the second particle, discarding 60% of the trajectories from the first located tracer will make a significant difference to the ratio of signal (from the second tracer) to noise (from the first tracer) (here signal/noise = 1/0.4) for the second tracer; therefore, the second tracer can be located properly from the majority of trajectories of the second tracer; if the data logging rate of the first particle is significantly higher than that of the second particle, only discarding more could make the same ratio of signal to noise for the second tracer.

To remove the trajectories safely, the function of the optimum fraction for discarding trajectories can be derived from an exponential approximation to the curve in Figure 8 as follows

$$\beta = -1.677\, e^{-1.631\frac{m}{n}} + 0.9278 \tag{17}$$

where m and n are the numbers of trajectories for the first and the second tracers in their located positions, respectively, and β is the optimum fraction for discarding trajectories.

Tracking for moving particles

Example 2: Two Moving Particles. Two tracers were fixed on two turntables, respectively, at a radius of 106 mm. The turntables were placed with approximate central symmetry in the field of view of the detectors as shown in Figure 9, rotating at a constant speed for each run. The rotating speeds of the turntables varied from 2 to 45 rpm; and the particle speeds varied from 22 to 500 mm/s for different runs. Each run took 10 min for data collection. To identify the tracers with different separation distances, the turntables were rotating at opposite orientations. The separation distance varied from 5 to 217 mm. The tracers used were the same as in Example 1. The tracers used had initial radioactivity: Tracer 1, 210 μCi, and Tracer 2, 100 μCi.

The sample size varied as the rotating speed of turntables increased, and was calculated by Eq. 3. For example, at a speed of 22 mm/s, the sample size was taken 290 events for the weaker tracer using Eq. 3; because the radioactivity ratio of the stronger to the weaker tracers was 2.1, the sample size was 610 events (=2.1 $\times$ 290) for the stronger tracer, thus the total sample size selected was 900 events (=290 + 610) at a speed of 22 mm/s. In a same way, the sample size was selected as 270 events for the two tracers at a speed of 500 mm/s. The tracers were located 60 times/s at a speed of 500 mm/s, and 10 times/s at a speed of 22 mm/s.

Figure 10 shows location data for particles 1 and 2 on turntables rotating in the xyz space at 25 rpm over a 30-s period, respectively. Figure 11 shows the results of location error and speed error for the two moving particles, respectively.

The results show that the errors of location and speed increased with the turning speed. But the rms location and speed errors are only 9 mm and 48 mm/s (less than 10%), respectively, at a speed up to 500 mm/s. Therefore, the improved Multiple-PEPT can be applied to the investigation of relative motions and interactions of particles.

An Example of Application to a Real System

This section will give an example for visualization of the relative motions of solids in a fluidized bed using the improved Multiple-PEPT technique. The solid mixing and dispersion can be monitored through the observation of the displacement between the two tracked particles. The experiments were carried out in a gas-solid fluidized bed, which consisted of a Plexiglas cylindrical column of 152-mm inner diameter and 1000-mm height. Air at ambient temperature was injected into the bed through a conical section, passing

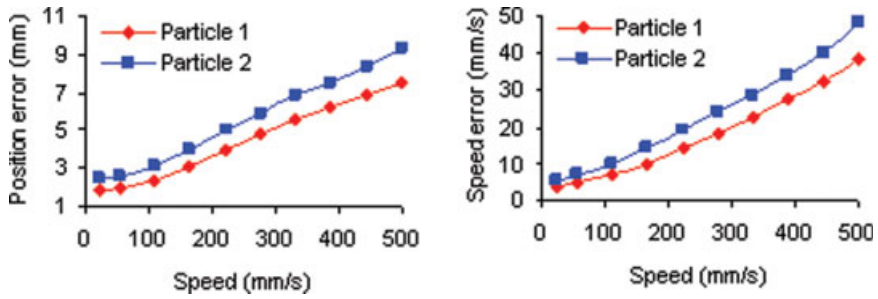

Figure 11. Location and speed errors of Particles 1 and 2.

[Color figure can be viewed in the online issue, which is available at www.interscience.wiley.com.]

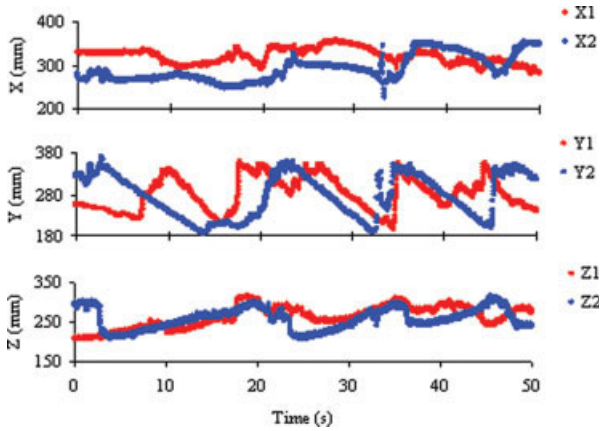

Figure 12. Trajectories of two particles tracked simultaneously at a superficial gas velocity of 0.31 m/s.

[Color figure can be viewed in the online issue, which is available at www.interscience.wiley.com.]

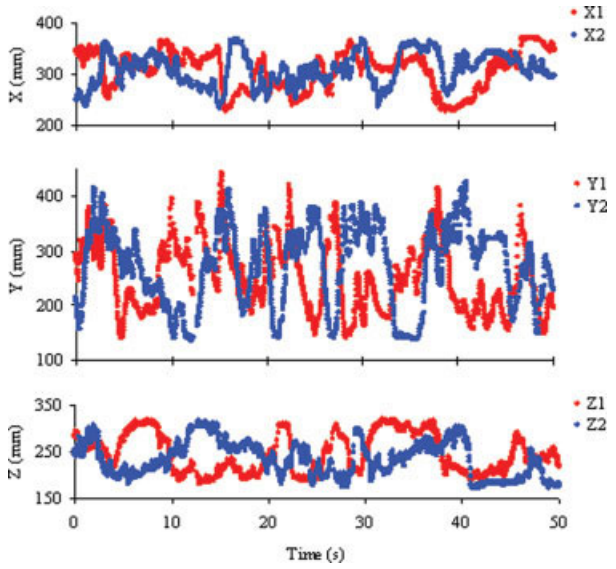

Figure 14. Trajectories of two particles tracked simultaneously at a superficial gas velocity of 0.48 m/s.

[Color figure can be viewed in the online issue, which is available at www.interscience.wiley.com.]

through a stainless steel porous plate and an air distributor, which supported the bed. The air was supplied by a GA11CFF air compressor. The flow rate was measured and controlled with calibrated rotameters. The experimental material was polyethylene with a size range from 300 to 1500 μm. The tracer particles were selected from the experimental bulk and their sizes were $\sim$1000 μm. Two particles were radioactively labeled using ^{18}F through surface modification techniques,[1,2] with 160 and 340 μCi of radioactivity, respectively. The experiments were carried out in a bubbling regime at superficial gas velocities of 0.31 and 0.48 m/s. The sample sizes were 1000 and 750 events at superficial gas velocities of 0.31 and 0.48 m/s, respectively. Each experiment took 1 h for the data collection. The results are shown in Figures 12–16.

As well known, bubbling fluidized beds have been shown to be an effective means of providing good mixing, as well as good heat and mass transfer. These features are achieved mainly due to solids circulating within the bed. The circulation transports particles around, therefore inducing the displacement or drift of particles in both the ascending flow and the return flow. This displacement between particles, which can be directly recorded through the improved Multiple-PEPT, can provide valuable data for analysis of many phenomena within a flourished bed, such as flow structure, particle collision, and segregation if a binary solid mixture is used.

Figures 12–15 present the relative motions of two polyethylene particles in a Plexiglas bed. Figure 16 shows histograms of the displacements between two polyethylene particles at superficial gas velocities of 0.31 and 0.48 m/s, respectively, over a period of 1 h. The results indicate that the relative motion between two labeled polyethylene particles varied greatly with the gas velocity. At a superficial gas velocity of 0.31 m/s, the trajectories of the two labeled particles were quite smooth. They were almost parallel and the displacement between the two particles changed slightly in the return flow (Figures 12 and 13). A significant change in the displacement can be observed only when the particles ascended with air bubbles and in the splash zone. This means that solids move mainly in a block or a cluster in the return flow at a low gas velocity. When the superficial gas velocity increased to 0.48 m/s, the solids within the bed moved more chaotically (Figures 14 and 15). Beside the main circulation, many local circulations can be seen from the trajectories, particularly in the ascending flow and the splash zone. These

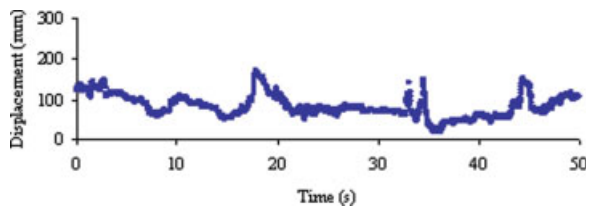

Figure 13. Displacements between two polyethylene particles as a function of time at a superficial gas velocity of 0.31 m/s.

[Color figure can be viewed in the online issue, which is available at www.interscience.wiley.com.]

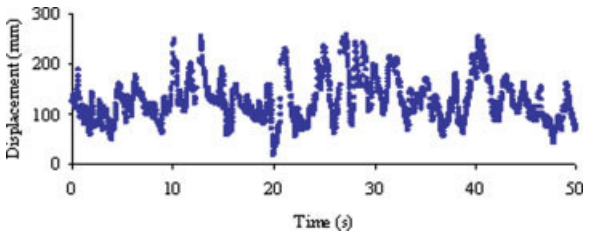

Figure 15. Displacement between two polyethylene particles as a function of time at a superficial gas velocity of 0.48 m/s.

[Color figure can be viewed in the online issue, which is available at www.interscience.wiley.com.]

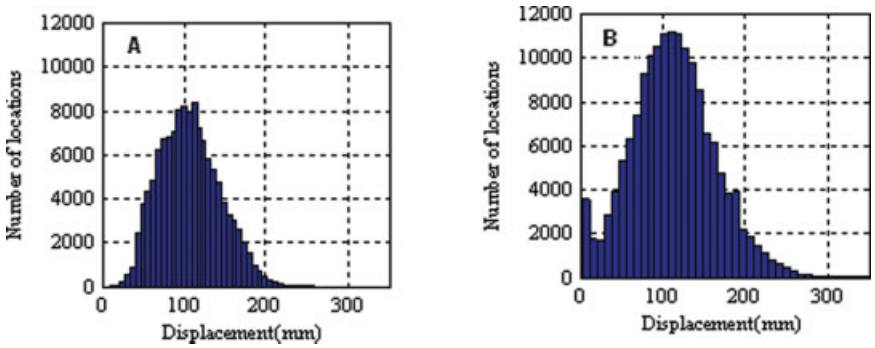

Figure 16. A and B show the histograms of the displacement between two polyethylene particles at superficial gas velocities of 0.31 and 0.48 m/s, respectively, over a period of 1 h (A: 0.31 m/s, B: 0.48 m/s).

[Color figure can be viewed in the online issue, which is available at www.interscience.wiley.com.]

circulations induced a significant change in the displacement between the two particles. If we define that the adjacent particles have been dispersed in the bed when the displacement between the two tracked particles is larger than two-third of the bed diameter or half of the bed height, the frequency for making this displacement can be used to estimate solid dispersion or mixing within the bed. Based on the relative motion of the two tracked particles, their position exchange frequency of the two particles increased from 0.1 to 0.58 Hz, the maximum displacement increased from 258 to 350 mm, and the standard deviation of the displacement increased from 36 to 50 mm, as shown in Figures 16A, B, when the gas velocity was increased from 0.31 to 0.48 m/s. These indicate that the solid dispersion within the bed increases significantly with the superficial gas velocity.

It might be noted that there are few jumps in Figures 14 and 15. As described above, the ability to locate the particle accurately is reduced towards the edges of detectors because the overall data rate falls and the quality of the data becomes poorer. However, the tracers can be located accurately over most of the field of view.

Conclusions

An improved Multiple-PEPT technique has been successfully developed. The technique can be used to track multiple freely moving particles, and to provide the relative motions of particles at a speed up to 500 mm/s within realistic engineering systems. The procedure is relatively simple and can be implemented to obtain a better understanding of physical processes for fundamental research as well as industrial applications.

For tracking a moving particle, the tracers are identified based on the numbers of their trajectories converted to their equivalents at the center of the field of view of the detectors. The tracking accuracy of a moving particle can be enhanced by selecting a suitable sample size for location calculation. The optimum sample size varies with the tracer speed and radioactivity. When the tracer speed is high, a small sample size will give more locations to smooth the motion trajectory. If a tracer has a higher radioactivity, the γ-ray events generated in the same period is larger; the optimum sample size therefore can be bigger to get more accurate locations.

Acknowledgments

The authors gratefully acknowledge the financial support from the EPSRC for this work and the Birmingham positron imaging camera.

Literature Cited

1. Fan X, Parker DJ, Smith MD. Labelling a single particle for positron emission particle tracking using direct activation and ion-exchange techniques. *Nucl Instrum Methods Phys Res A*. 2006;562:345–350.
2. Fan X, Parker DJ, Smith MD. Enhancing ^{18}F uptake in a single particle for positron emission particle tracking through modification of solid surface chemistry. *Nucl Instrum Methods Phys Res A*. 2006;558:542–546.
3. Bemrose CR, Fowles P, Hawkesworth MR, O'Dwyer MA. Application of positron emission tomography to particulate flow measurement in chemical engineering processes. *Nucl Instrum Methods Phys Res A*. 1988;273:874–880.
4. Parker DJ, Broadbent CJ, Fowles P, Hawkesworth MR, McNeil PA. Positron emission particle tracking—a technique for studying flow within engineering equipment. *Nucl Instrum Methods Phys Res A*. 1993;326:592–607.
5. Parker DJ, Broadbent CJ, Fowles P, Hawkesworth MR, McNeil PA. Positron emission tomography for process applications. *Meas Sci Technol*. 1996;7:287–296.
6. Parker DJ, Allen DA, Benton DM, Fowles P, McNeil PA, Tan M, Beynon TD. Developments in particle tracking using the Birmingham Positron Camera. *Nucl Instrum Methods Phys Res A*. 1997;392:421–426.
7. Parker DJ, Dijkstra AE, Martin TW, Seville JPK. Positron emission particle tracking studies of spherical particle motion in rotating drums. *Chem Eng Sci*. 1997;52:2011–2022.
8. Parker DJ, Forster RN, Fowles P, Takhar PN. Positron emission particle tracking using the new Birmingham positron camera. *Nucl Instrum Methods Phys Res A*. 2002;477:540–545.
9. Knight PC, Johansen A, Kristensen KG, Schæfer T, Seville JPK. An investigation of the effects on agglomeration of changing the speed of a mechanical mixer. *Powder Technol*. 2000;110:204–209.
10. Kuo HP, Knight PC, Parker DJ, Tsuji Y, Adams MJ, Seville JPK. The influence of DEM simulation parameters on the particle behaviour in a V-mixer. *Chem Eng Sci*. 2002;57:3621–3638.
11. Bakalis S, Cox PW, Wang-Nolan W, Parker DJ, Fryer PJ. Use of positron emission particle tracking (PEPT) technique for velocity measurements in model food fluids. *J Food Sci*. 2003;68:2684–2692.
12. Bakalis S, Cox PW, Fryer PJ. Measurement of velocity distributions of viscous fluids using positron emission particle tracking. In: *Ninth Int. Congress on Eng. and Food*, Montpellier, France, March 7–11, 2004.
13. Fairhurst PG, Barigou M, Fryer PJ, Pain J-P, Parker DJ. Using positron emission particle tracking (PEPT) to study nearly neutrally buoyant particles in high solid fraction pipe flow. *Int J Multiphase Flow*. 2001;27:1881–1901.

14. Fangary YS, Barigou M, Seville JPK, Parker DJ. A Lagrangian study of solids suspension in a stirred tank vessel by positron emission particle tracking (PEPT). *Chem Eng Technol*. 2002;25:521–528.
15. Barigou M, Fairhurst PG, Fryer PJ, Pain J-P. Concentric flow regime of solid-liquid food suspensions: theory and experiment. *Chem Eng Sci*. 2003;58:1671–1686.
16. Cox PW, Fryer PJ. Heat transfer to foods: modelling and validation. *J Therm Sci*. 2002;11:320–330.
17. Cox PW, Bakalis S, Ismail H, Forster R, Parker DJ, Fryer PJ. Visualisation of three-dimensional flows in rotating cans using positron emission particle tracking (PEPT). *J Food Eng*. 2003;60:229–240.
18. Bertrand F, Leclaire LA, Levecque G. DEM-based models for the mixing of granular materials. *Chem Eng Sci*. 2005;60:2517–2531.
19. Cooper S, Coronella CJ. CFD simulations of particle mixing in a binary fluidized bed. *Powder Technol*. 2005;151:27–36.
20. Santomaso A, Olivi M, Canu P. Mixing kinetics of granular materials in drums operated in rolling and cataracting regime. *Powder Technol*. 2005;152:41–51.
21. Conway SL, Lekhal A, Khinast JG, Glasser BJ. Granular flow and segregation in four-bladed mixer. *Chem Eng Sci*. 2005;60:7091–7107.
22. Santomaso A, Olivi M, Canu P. Mechanism of mixing of granular materials in drum mixers. *Chem Eng Sci*. 2004;59:3269–3280.
23. Fishwick RP, Winterbottom MJ, Stitt EH. Effect of gassing rate on solid–liquid mass transfer coefficients and particle slip velocities in stirred tank reactors. *Chem Eng Sci*. 2003;58:1087–1093.
24. Yang Z, Parker DJ, Fryer PJ, Bakalis S, Fan X. Multiple-particle tracking—an improvement for positron particle tracking. *Nucl Instrum Methods Phys Res A*. 2006;564:332–338.

Manuscript received Oct. 26, 2006, and revision received May 9, 2007.